3D Focusing Acoustic Lens Optimization Method Using Multi-factor and Multi-level Orthogonal Test Designing Theory

Hongyu Sun[1], Shen Wang[1], Songling Huang[1], Lisha Peng[1], Qing Wang[2], Wei Zhao[1], and Jun Zhou[1]

[1]Department of Electrical Engineering, Tsinghua University, Beijing, China
[2]Department of Engineering, Durham University, Durham, UK

Corresponding author: Songling Huang (email: huangsling@tsinghua.edu.cn)

This research was supported by the National Key R&D Program of China (Grant No. 2018yff01012802), National Natural Science Foundation of China (NSFC) (No. 51677093) and National Natural Science Foundation of China (NSFC) (No. 51777100).

ABSTRACT Focusing systems that consist of acoustic lenses exhibit higher controllability and focusing intensity when manipulating sound waves. Different parameters have different effects on the performance of the acoustic lens, so analyzing a variety of parameter combinations for the acoustic lens is difficult because of the complexity of the test. Therefore, we report an analytical method for studying the focusing performance of different factors on acoustic lenses at different levels, and the influence degree of each factor is investigated through range analysis. Results show that the factors that have the most significant influence on the focusing intensity, focal-area dimensions, and focal length are the incident sound field's pressure P0, cell dimension c, and cell edges k, respectively. Moreover, the effects of other parameters, including the biased incident-wave angles, are obtained and analyzed through finite-element simulations. After analyzing and comprehensively comparing the influences of various parameters, the optimal parameter combination is obtained to achieve the best focusing performance of an acoustic lens. The experimental results show that the focusing intensity of the optimized acoustic lens is nearly 90% higher than the non-optimized one, which proves the effectiveness of the orthogonal test-optimization method in this paper.

INDEX TERMS Acoustic lens, focusing intensity, orthogonal test, focal area dimensions

I. INTRODUCTION

When a sound wave is used as an information carrier or energy-orientation method, its energy gradually attenuates during propagation. Therefore, we must use different technical methods to focus sound waves to efficiently utilize sound energy [1-5]. Acoustic lenses can focus the energy of sound waves in a relatively small space, which is a region with high energy density. Acoustic focusing that is achieved by acoustic lenses has higher efficiency and controllability than self-focusing and phased-array-focusing methods [6-9]. Therefore, acoustic lenses are widely used in the field of non-destructive testing (NDT) and medical treatment [10-13]. As the accuracy of non-destructive testing and the resolution requirements of medical ultrasound imaging have increased in recent years, the focusing intensity, accuracy, and control capabilities of acoustic lenses have also been improved [14-19].

According to the literature in the field of ultrasonic composite acoustic lenses, different cell shapes and structures have been studied to improve the focusing performance of the lens, including rigid cylinders [20-23], Helmholtz resonators [24-26], cross structures [27-29] and concentric rings [30]. In a study of a rigid cylindrical acoustic lens that was based on the genetic algorithm and Bragg reflection [31], A. Hakansson simulated acoustic lenses of different sizes, frequencies, and focal lengths by changing the arrangement and combination of rigid cylinders in space [32]. This paper concluded that high frequency and small focal length could increase the focusing capability of acoustic lenses. Although a rational arrangement of rigid cylinders can effectively control the propagation direction and focal position of acoustic waves, such a lens structure cannot achieve three-dimensional focusing, and the total volume fraction is large, which increases the difference between the acoustic impedance and the medium. Therefore, the focusing performance of an acoustic lens with rigid cylinders is relatively weak. Helmholtz resonators, which are a component of acoustic lenses, have a broader effective refractive index and can reduce the impedance mismatch compared to a rigid cylindrical acoustic lens. Although

a Helmholtz-lens structure has been proven to exhibit better-focusing capability and a smaller focusing length, its complex asymmetric structure poses difficulties during precision machining in actual manufacturing.

In a study of unit cell shapes, Dennis Li used the shape of different scattering elements as a variable parameter based on the genetic algorithm to obtain the expected high refractive index and low impedance mismatch [33]. However, the optimized acoustic lens structure that is obtained from this genetic algorithm is relatively complicated and can only be used in experiments through mandatory approximation. Moreover, a "+"-shaped cross (CS) cell structure has high effective density and low total volume fraction, so higher focusing intensity and lower impedance mismatch can be achieved [34]. A recent study showed that cross-shaped single-phase units with subwavelength size could successfully achieve 3D underwater focusing because of anisotropic dispersion in the first band [29]. Although such an acoustic-lens structure can achieve three-dimensional focusing, whether the structure of the acoustic lens is optimal considering various parameters was-not studied. From the existing literature, the effects of different parameters on the performance of acoustic lenses have not been fully investigated, even though the structures of acoustic lenses have been continually improved to increase their focusing capabilities. Furthermore, the dimensions of the focal area should be reduced to meet the requirements of high-precision defect detection and tumor treatment. Therefore, we must comprehensively consider the optimal sound-field intensity, focal-area dimensions, and focal length of acoustic lenses under a combination of different influencing factors.

In this work, the influence degree of design parameters is investigated to improve the performance of an acoustic lens. The eight selected parameters of the lens are the lattice constant a, cell dimensions b and **c**, concave depth r, cell edges k (triangular, quadrilateral, and hexagonal structures), frequency f, incident sound pressure P_0, and lens height h_l. Besides, the test results are the wave intensity M, effective horizontal width L_h, effective vertical width L_v, and focal length l_F. The outline of this work is as follows. First, the configuration of different acoustic-lens structures is proposed, and simulation analysis with the finite-element method (FEM) is performed for triangular, quadrilateral, and hexagonal cell structures. Next, an $L_{27}(3^8)$ orthogonal table is determined according to the selected parameters and levels, and the range analysis is processed by using the above simulation method; thus, the effects of different parameters on the wave intensity, effective horizontal width, effective vertical width, and focal length can be obtained. Then, the effect of the incident wave's angle is studied, and the optimal combination of parameters is selected through a comprehensive analysis of the orthogonal test results. Finally, the focusing performance of the optimized acoustic lens is verified by experiments.

II. CONFIGURATION AND SIMULATION ANALYSIS

A. CONFIGURTAION OF ACOUSTIC LENS

Since the acoustic lens aims to have good focusing performance, high effective densities, and low effective bulk modulus are required [28]. For an acoustic lens, the size and structure of the unit cell, as well as the cells' arrangement, will affect the characteristics of the lens. In this work, the unit cells of the triangular, quadrilateral, and hexagonal concave-cross (CC) structures are used to analyze the effect of different cell structures on the focusing capability of the acoustic lens, as shown in Fig. 1.

Figs. 1(a-c) show different cell structures, where a is the lattice constant, b and c are the cell dimensions, r is the concave depth. Although the side length is set to $a/2$ for a hexagonal unit cell, its average size is still approximately a, similar to those for other cell structures. Fig. 1(d-f) show the arrangement of the cells, and Fig. 1(g-i) are the 3D model of the acoustic lenses, where h_l is the lens height.

B. SIMULATION ANALYSIS

To investigate the performance for different lenses, COMSOL software is used to simulate the distribution of the sound pressure, which was theoretically proposed and experimentally verified previously [27]. The conservation of momentum and mass equations utilized in the simulation are shown as follows [35].

$$-j\omega\boldsymbol{\rho}(\boldsymbol{r})\rho_0\boldsymbol{v} = \nabla p\,, \tag{1}$$

$$-B(\boldsymbol{r})B_0\nabla\cdot\boldsymbol{v} = j\omega p\,, \tag{2}$$

where v is the velocity vector, p is the wave pressure, $B(r)$ is the relative bulk modulus and ρ is the relative density tensor. For simplification purposes, B_0 and ρ_0 use the parameters of water. The incident wave is applied as the plane wave that propagates along the x-direction in the simulation. The press ure acoustics, frequency domain interface is used to simulated the sound field, and sound hard boundary is used where the normal component of the acceleration (and thus the velocity) is zero. In the experiment, a point source is used to generate spherical waves and placed 200 mm away from the composite lens. The spherical waves can be approximated as plane waves when $k_r \gg 1$, which was proved by the experimental approximation [29]. To avoid the wave reflection from the boundaries, Perfect Matching Layers (PMLs) are utilized on the boundaries of the model. Also, the thermal effect and fluid flow of low-viscosity fluids can be omitted because the propagation medium of ultrasound is quasi-static water.

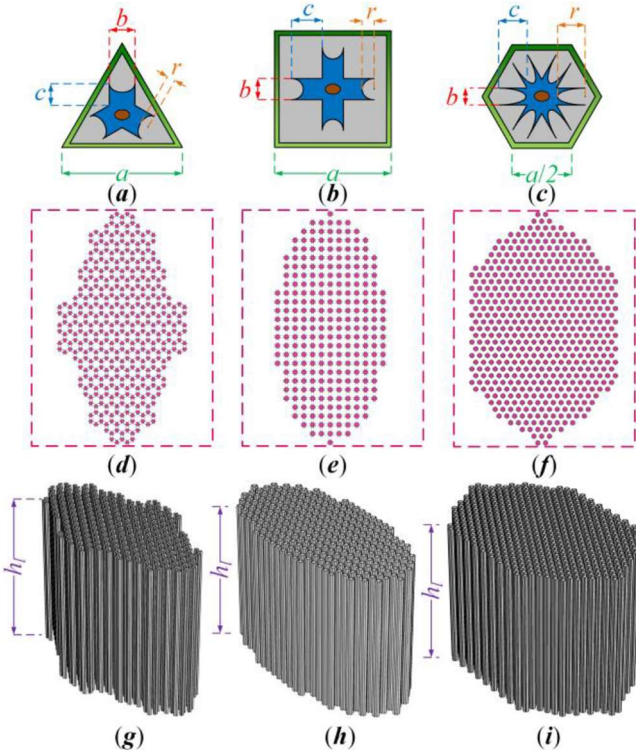

FIGURE 1. Configurations of acoustic lenses. (a, d, g) are the structure, arrangement and 3D model for a triangular CC cell, respectively; (b, e, h) are the structure, arrangement and 3D model for a quadrilateral CC cell, respectively; (c, f, i) are the structure, arrangement and 3D geometric model for a hexagonal CC cell, respectively.

Figs. 2(a-c) show the simulation results for three cell structures, and the same legend color bar is used to represent the sound field intensity values of different lens structures. To achieve a valid comparison of the sound fields for different lens structures, the other variables in the simulation are fixed as: a=12 mm, b=2 mm, c=2 mm, r=0.8c, frequency f=20 kHz, P_0=10 Pa, and h_l=500 mm. For the definition of the coordinate axis, the horizontal symmetry axis of the acoustic lens is set to the x-axis direction, and the vertical symmetry axis of the acoustic lens is set to the y-axis direction. Moreover, the center of the acoustic lens is set to the origin of the coordinates. The plane waves with a sound pressure of P_0 are incident from the left side of the acoustic lens along the positive direction of the x-axis. The single unit cell on the left is a partially enlarged view of the green dotted line of the acoustic lens in Fig. 2. Fig. 2(c) shows that the hexagonal CC structure has the best focusing capability of sound waves.

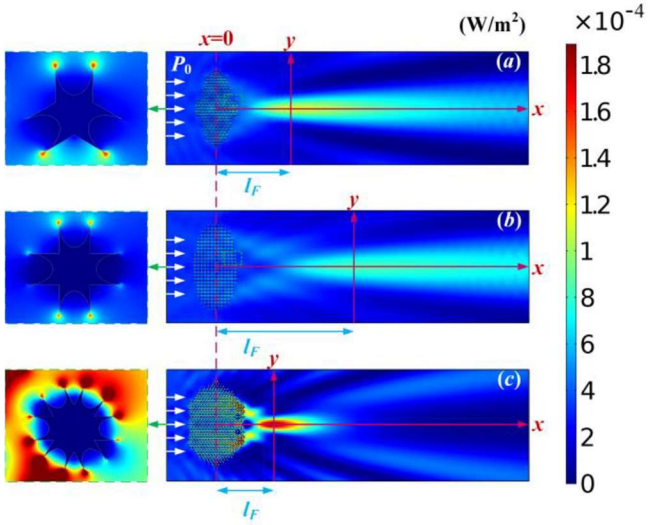

FIGURE 2. Wave intensity distributions for different lens structure: (a) lens with triangular CC cells; (b) lens with quadrilateral CC cells; (c) lens with hexagonal CC cells.

Wave intensity distributions of Fig. 2(a-c) along x and y axis are shown in Fig. 3(a, b), and k=3, 4 and 6 refer to triangular, quadrilateral and hexagonal CC cell, respectively. It can be seen that the hexagonal CC structure with a peak value of 1.89×10-4 W/m^2 has the highest focusing intensity, and the triangular CC structure (1.11×10-4 W/m^2) and the quadrilateral CC structure (0.84×10-4 W/m2) follow in order. Moreover, the focal length l_F of the acoustic lens is defined as the distance from the center of the acoustic lens to the highest sound field intensity position. Therefore, the focal lengths for different lens structures can be obtained. Since the sound field inside the acoustic lens has a strong oscillation, it is then omitted in Fig. 3(a). In this work, the effective focal area dimensions are defined as the area with the wave intensity higher than 80% peak value, which is shown as the gray areas in Fig. 3(a, b). The effective horizontal width Lh is shown in Fig. 3(a), and the effective vertical width Lv is shown in Fig. 3(b). Therefore, the peak wave intensity, focal area dimensions, and the focal length can be obtained in the simulation.

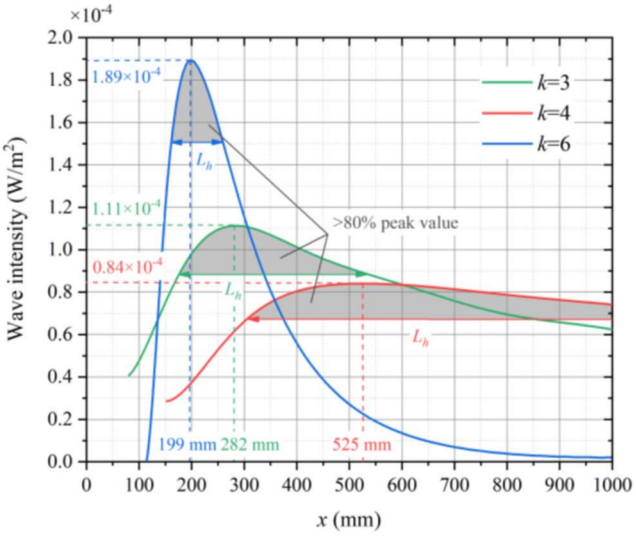

(a)

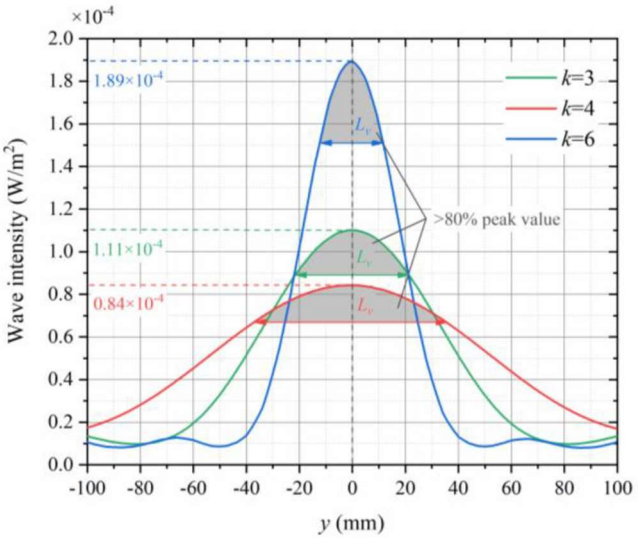

(b)

FIGURE 3. Wave intensity distributions along (a) x-axis; (b) y-axis, and *k*=3, 4 and 6 refer to triangular, quadrilateral and hexagonal CC cell, respectively. Areas greater than 80% of the peak are indicated in gray, and the effective horizontal width is L_h, the effective vertical width is L_v.

III. ORTHOGONAL TEST AND ANALYSIS

A. TEST DESIGN

Orthogonal test design refers to a design method that studies multi-factors and multi-levels. Based on the orthogonality, some representative points are selected from the comprehensive test, and these representative points were uniformly dispersed and neatly comparable. [36] The orthogonal table is used as the primary tool of the orthogonal test, and its selection depends on the number and level of factors in the test, then the representative points are selected from comprehensive tests. The method of replacing large-scale tests with very few tests will significantly improve the efficiency of scientific analysis [37]. Therefore, as an effective multi-factor experimental design method, the orthogonal test method is chosen in this paper to analyze the focusing performance for acoustic lenses with different structures.

Of all the impact factors, lattice constant a, cell dimension b, cell dimension c, concave depth r, lens height h_l and cell edges k are selected because the cell structure will strongly affect the focusing capability of an acoustic lens, and other external factors such as frequency f and incident wave pressure P_0 are also considered. Levels of eight factors should be controlled within a reasonable range. The three levels of lattice constant a are 12, 14, and 16 mm, so the cell dimensions b and c should be less than or equal to 3 mm (1, 2, and 3 mm). In order to reasonably determine the concave size r, a proportional method is used and its levels are 0.6c, 0.8c and c. In this study, the focusing capability of three different acoustic lenses is studied. Different structures are defined by the number of cell edges k, which are 3, 4, and 6. To obtain the working frequencies, the band structure of each lens is calculated by the eigenvalue analysis using FEM according to the Floquet- Bloch theorem [38]. Therefore, working frequencies below 50 kHz can be selected, so the three levels of frequency f are 16, 20 and 24 kHz. Moreover, the three levels of incident wave pressure P_0 are 5, 10 and 15 Pa, and the three levels of lens height h_l are 300, 400 and 500 mm. As discussed above, an $L_{27}(3^8)$ orthogonal table including eight factors and three levels is shown in Table I.

TABLE I
FACTORS AND LEVELS OF THE ORTHOGONAL TEST

No.	Factors	Level 1	Level 2	Level 3
A	Lattice constant a (mm)	12	14	16
B	Cell dimension b (mm)	1	2	3
C	Cell dimension c (mm)	1	2	3
D	Concave depth r (mm)	0.6c	0.8c	1c
E	Cell edges k	3	4	6
F	Frequency f (KHz)	16	20	24
G	Incident pressure P_0 (Pa)	5	10	15
H	Lens height h_l (mm)	300	400	500

For an acoustic lens, a maximum sound intensity, a minimum focal area, and a suitable focal length are always expected. Because a higher sound intensity is beneficial to high-resolution imaging and high-efficiency medical treatment, which are the main applications of the acoustic lens. Moreover, a larger focal area will reduce defect identification accuracy in non-destructive testing (NDT). Also, the requirement for focal lengths of acoustic lenses is different in specific applications. Therefore, the wave intensity M, effective horizontal width L_h, effective vertical width L_v and focal length l_F are selected as the results for the orthogonal test.

B. RESULTS AND RANGE ANLYSIS

Based on the simulation method and the $L_{27}(3^8)$ orthogonal table, results are calculated and obtained in Table II. By analyzing the results of these 27 orthogonal tests, it is possible to replace all of the 6561 tests. To evaluate the influence degree

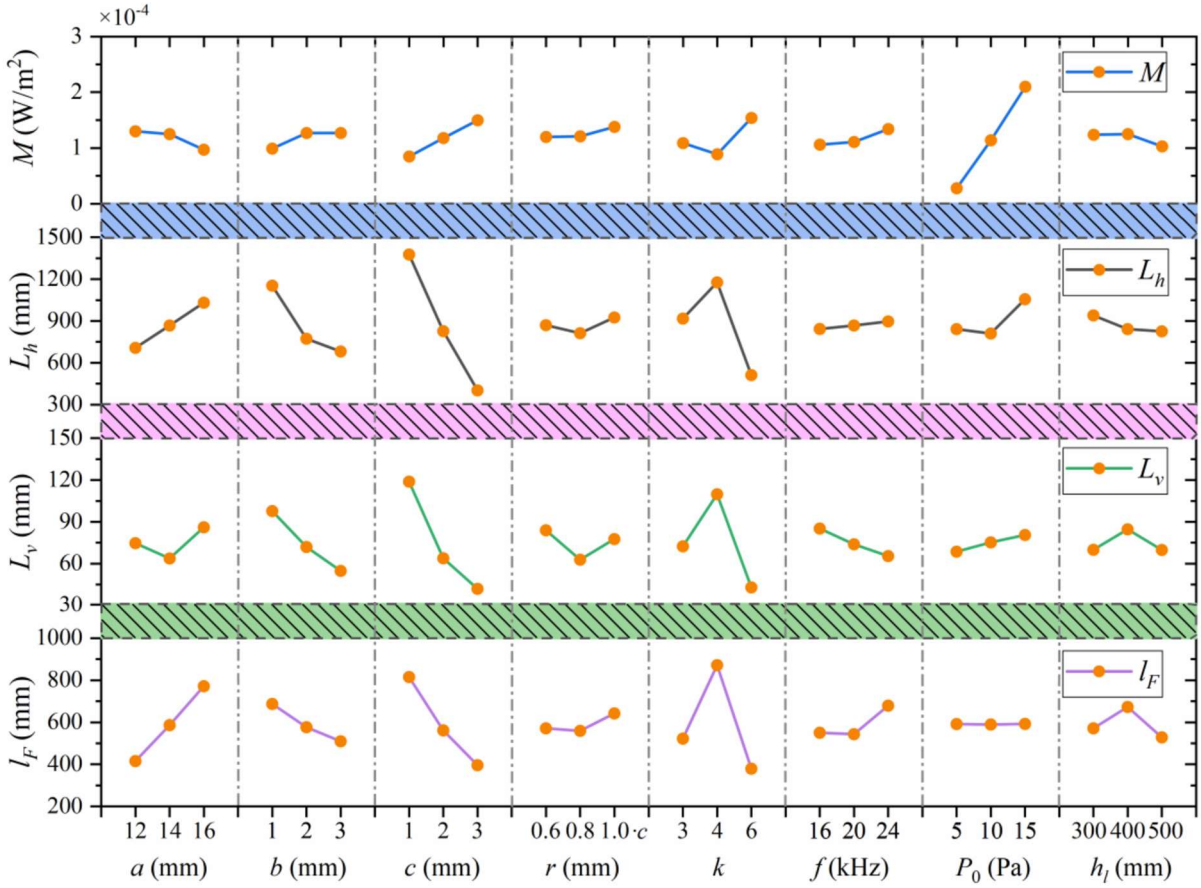

FIGURE 4. The average value of per level for each factor.

of nine factors on test results, a range analysis of the orthogonal method is necessary. In the calculation of the range analysis, the average K_{zn} and the influence degree T_z are shown.

$$k_{ZN} = \frac{1}{m}\sum_{i=1}^{n} y_{Zi}\,, \tag{3}$$

$$T_Z = R_{\max Z} - R_{\min Z}\,, \tag{4}$$

where i is the test number; Z represents the impact factor; y is the test result, which is the signal intensity; n=27; m=9; N is the level number. $Rmax_Z$=max{k_{Z1}, k_{Z2}, k_{Z3}}, $Rmin_Z$=min{k_{Z1}, k_{Z2}, k_{Z3}}. In the range analysis, the average value k_{ZN} when N=1, 2, 3 describes the effect of the factor Z on the test result M. Moreover, the influence degree T_Z represents how large the impact of factor Z is. Using the analysis method above, the range analysis result with different k_{ZN} and T_Z are shown in Table III.

It is shown in Table III that the range analysis is implemented at different factors and levels. In order to facilitate comparative analysis, Fig. 4 shows the average value of each factor at each level for different test results and Fig. 5 shows the influence degree for different factors at different results. It should be noted that the influence degrees are normalized based on the maximum value of each result. In Fig. 5, the top three factors that affect the wave intensity M are: incident wave pressure P_0, cell dimension c and cell edges k. The incident sound field pressure P_0, as the most influential factor, has a dominant effect on the focusing intensity of an acoustic lens. In addition, c and k share a similar impact. It is shown in Fig. 4 that P_0 is proportional to M, and c also increases with M, and $M_{k=6}>M_{k=3}>M_{k=4}$. Because with the increase of k, the omnidirectional symmetry of each unit cell increases, which reduces the energy loss of acoustic field caused by the inclined incident wave angle.

In Fig. 5, for effective horizontal width L_h, the results show that $T_C>T_E>T_B$. The cell dimension c has the largest effect, k and b follow in order. Fig. 4 shows that L_h and b decrease with the increase of c, while $L_{h,k=4}>L_{h,k=3}>L_{h,k}$=6. For effective vertical width L_v, Fig. 5 depicts that $T_C>T_E>T_B$, which is the same as that of L_h, as well as the effect of factor levels.

We can see from Fig. 5 that $T_E>T_C>T_A$ under the result of the focal length l_F. The cell edge k has the largest effect, while c and lattice constant a follow in order. As observed in Fig. 4, the average value for each level shows that the focal length decreases with the increase of c, and increases with a. For cell edge, we can see that $l_{F,k=4}>l_{F,k=3}>l_{F,k}$=6.

C. EFFECT OF INCIDENT ANGLE

In the practical applications, the incident sound waves are not always parallel along the central axis of the lens, and there

may be an offset angle. This angular offset will cause the positional shift of the focal point, as well as the change in the sound focusing intensity, thereby affecting the performance of the acoustic lens. In general, the focal position always changes in accordance with the change in the wave incident angle. Therefore, it is necessary to analyze the change of the focusing intensity of the sound field at different incident angles. In this work, the gain and loss percentage of the peak wave intensity are studied at an incident angle is 30 ° when compared with unbiased incident waves.

Fig. 6 shows the simulation results at different k (=3, 4, 6) and r (=1.2, 1.6, 2 mm), and keeps other factors as constants: a=12 mm, b=2 mm, c=2 mm, f=20 k_{Hz}, P_0=5 Pa, and h_l=500 mm. The two factors k and r are selected because the acoustic lens composed of different unit cell structures will have different effects on the biased incident wave. Moreover, the size of r affects the total volume fraction, so it dominates the transmission efficiency of acoustic energy. It is observed that the peak value of the wave intensity increases when k=4 and 6. However, for k=3, the biased incident waves will reduce the focusing intensity. Moreover, when r increases, the peak intensity decreases for all cell edges k. Therefore, the hexagonal CC structure acoustic lens can focus the waves when a biased incident angle exists, even better than an unbiased one. Also, the concave depth r should be as small as possible to prevent focal intensity loss when the incident wave has a biased angle.

D. OPTIMAL COMBINATION OF PARAMETERS

According to the selection criteria of the orthogonal test, the factors with the highest influence degree should be selected with an appropriate level, and non-important factors can be arbitrarily selected. For the wave intensity M, to obtain a high value, the level of each factor should be: A_1(a=12 mm), B_3(b=3 mm), C_3(c=3 mm), D_3(r=1.0 c), E_3(k=6), F_3(f=24 k_{Hz}), G_3(P_0=15 Pa), H_2(h_l=400 mm). Considering the effective horizontal width L_h and vertical width Lv, the level of each factor should be: A_1(a=12 mm), B_3(b=3 mm), C_3(c=3 mm), D_1(r=0.6 c), E_3(k=6), F_3(f=24 k_{Hz}), G_3(P_0=15 Pa), H_3(h_l=500 mm). It shows that except for the factors D and H, the level selection for other factors remains the same for M, L_h, and L_v. For M, the top three impact factors are G, E, and C. And for L_h and L_v, the top three impact factors are C, E and B. Fig. 5 shows that the influence degrees for factors D and H under L_v are higher than those under M and L_h. Therefore, considering the above conditions including the biased incident waves, the level of each factor should be selected as: A_1(a=12 mm), B_3(b=3 mm), C_3(c=3 mm), D_1(r=0.6 c), E_3(k=6), F_3(f=24 kHz), G3(P_0=15 Pa), H_3(h_l=500 mm). The test under this certain level can be then considered as the optimized test.

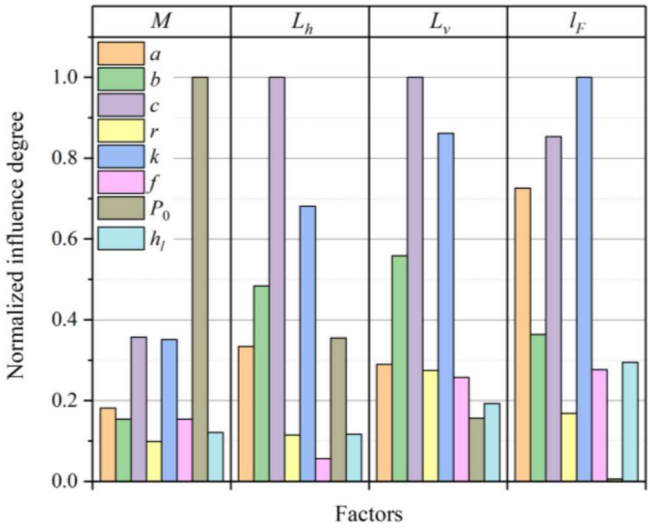

FIGURE 5. The influence degree of different results for each factor.

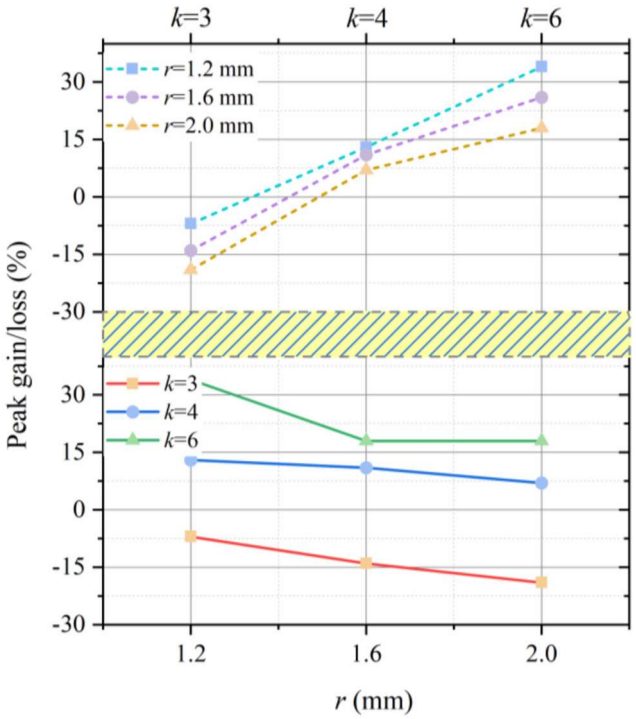

FIGURE 6. The change of the focusing intensity of the sound field under biased incident waves: the effect of factor *k* and *r*.

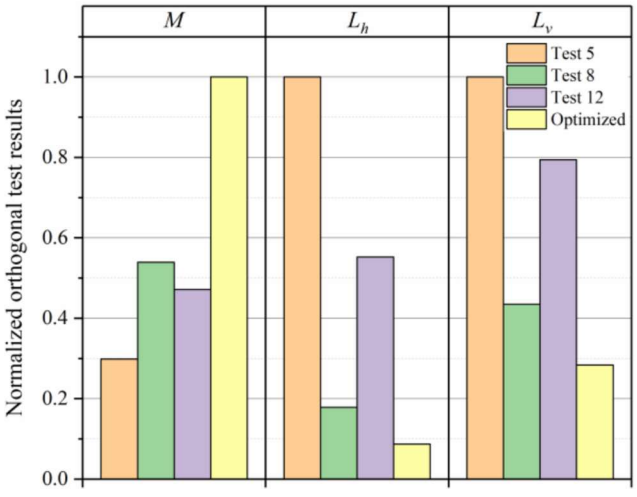

FIGURE 7. Normalized orthogonal test results for test No. 5, 8, 12 and the optimized one.

TABLE II
ORTHOGONAL DATA AND TEST RESULTS

Test No.	Factors								Results			
	A	B	C	D	E	F	G	H				
	a	*b*	*c*	*r*	*k*	*f*	P_0	h_l	*M*	L_h	L_v	l_F
	mm	mm	mm	mm	1	kHz	P_a	mm	($x10^{-4}$)			
1	12	1	1	0.6*c*	3	16	5	300	0.103	1500	150	519.5
2	12	1	1	0.6*c*	4	20	10	400	0.425	1500	228	1172
3	12	1	1	0.6*c*	6	24	15	500	1.93	1500	74	458
4	12	2	2	0.8*c*	3	16	5	400	0.231	558	59	301
5	12	2	2	0.8*c*	4	20	10	500	0.842	900	68	513
6	12	2	2	0.8*c*	6	24	15	300	3.23	79.6	19.5	201.3
7	12	3	3	1*c*	3	16	5	500	0.305	49.11	20.1	97.35
8	12	3	3	1*c*	4	20	10	300	1.52	160.7	29.55	250.3
9	12	3	3	1*c*	6	24	15	400	3.12	115	24	218.1
10	14	1	2	1*c*	3	20	15	300	1.477	1500	77.1	534
11	14	1	2	1*c*	4	24	5	400	0.189	1500	104.5	1161
12	14	1	2	1*c*	6	16	10	500	1.33	497	54	418.4
13	14	2	3	0.6*c*	3	20	15	400	3.009	308	39.6	311.5
14	14	2	3	0.6*c*	4	24	5	500	0.38	530	45.8	560
15	14	2	3	0.6*c*	6	16	10	300	1.7	81.42	26	198.75
16	14	3	1	0.8*c*	3	20	15	500	1.619	1500	81.9	566
17	14	3	1	0.8*c*	4	24	5	300	0.1769	1500	97.2	1144
18	14	3	1	0.8*c*	6	16	10	400	1.394	397	48.1	379.4
19	16	1	3	0.8*c*	3	24	10	300	1.157	637	50.3	570.5
20	16	1	3	0.8*c*	4	16	15	400	1.802	1500	106.6	950
21	16	1	3	0.8*c*	6	20	5	500	0.4646	243.5	35.3	403.4
22	16	2	1	1*c*	3	24	10	400	0.655	1500	120.08	1195
23	16	2	1	1*c*	4	16	15	500	1.129	1500	196.3	1138
24	16	2	1	1*c*	6	20	5	300	0.2184	1500	73.3	764.7
25	16	3	2	0.6*c*	3	24	10	500	1.261	713.1	53.5	599.5
26	16	3	2	0.6*c*	4	16	15	300	1.58	1500	106.7	952
27	16	3	2	0.6*c*	6	20	5	400	0.455	198.6	32.35	369.9

TABLE III
RANGE ANALYSIS FOR THE ORTHOGONAL TEST RESULTS

Results	Level	Factors							
		A	B	C	D	E	F	G	H
		a	*b*	*c*	*r*	*f*	*f*	P_0	h_l
	1	K_{A1}=1.30	K_{B1}=0.99	K_{C1}=0.85	K_{D1}=1.20	K_{E1}=1.09	K_{F1}=1.06	K_{G1}=0.28	K_{H1}=1.24
M	2	K_{A2}=1.25	K_{B2}=1.27	K_{C2}=1.18	K_{D2}=1.21	K_{E2}=0.89	K_{F2}=1.11	K_{G2}=1.14	K_{H2}=1.25
(10^{-4} MM)	3	K_{A3}=0.97	K_{B3}=1.27	K_{C3}=1.50	K_{D3}=1.38	K_{E3}=1.54	K_{F3}=1.34	K_{G3}=2.10	K_{H3}=1.03
	T_{X1}	0.33	0.28	0.65	0.18	0.64	0.28	1.82	0.22
	1	K_{A1}=707	K_{B1}=1153	K_{C1}=1377	K_{D1}=870	K_{E1}=918	K_{F1}=843	K_{G1}=842	K_{H1}=940
L_h	2	K_{A2}=868	K_{B2}=773	K_{C2}=827	K_{D2}=813	K_{E2}=1177	K_{F2}=868	K_{G2}=710	K_{H2}=842
(mm)	3	K_{A3}=1032	K_{B3}=682	K_{C3}=403	K_{D3}=925	K_{E3}=512	K_{F3}=897	K_{G3}=1056	K_{H3}=826
	T_{X2}	326	472	975	112	664	55	346	114
L_v	1	K_{A1}=1.30	K_{B1}=97.76	K_{C1}=118.8	K_{D1}=83.99	K_{E1}=72.40	K_{F1}=85.20	K_{G1}=68.62	K_{H1}=69.96
(mm)	2	K_{A2}=1.30	K_{B2}=71.95	K_{C2}=63.85	K_{D2}=62.88	K_{E2}=109.8	K_{F2}=73.90	K_{G2}=75.28	K_{H2}=84.69
	3	K_{A3}=1.30	K_{B3}=54.82	K_{C3}=41.92	K_{D3}=77.66	K_{E3}=42.95	K_{F3}=65.43	K_{G3}=80.63	K_{H3}=69.88
	T_{X3}	22.25	42.93	76.85	21.12	66.23	19.77	12.02	14.81
l_F	1	K_{A1}=1.30	K_{B1}=687	K_{C1}=815	K_{D1}=571	K_{E1}=522	K_{F1}=550	K_{G1}=591	K_{H1}=571
(mm)	2	K_{A2}=1.30	K_{B2}=576	K_{C2}=561	K_{D2}=559	K_{E2}=871	K_{F2}=543	K_{G2}=589	K_{H2}=673
	3	K_{A3}=1.30	K_{B3}=509	K_{C3}=396	K_{D3} =642	K_{E3}=379	K_{F3}=679	K_{G3}=592	K_{H3}=528
	T_{X4}	357	179	420	83	492	136	3	145

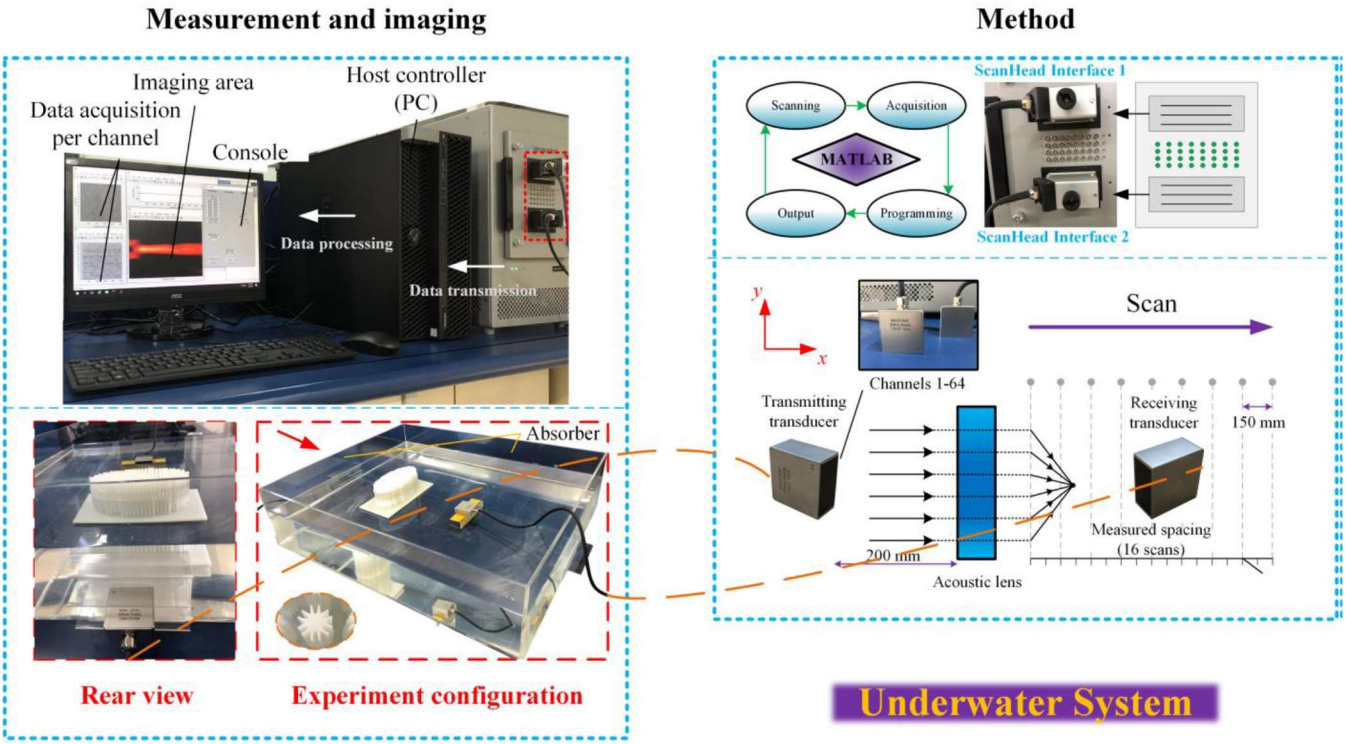

FIGURE 8. Experimental configuration of a 3D underwater ultrasound focusing system. Composite lenses with different cell shapes are fabricated using 3D printing technology (HORI Z300).

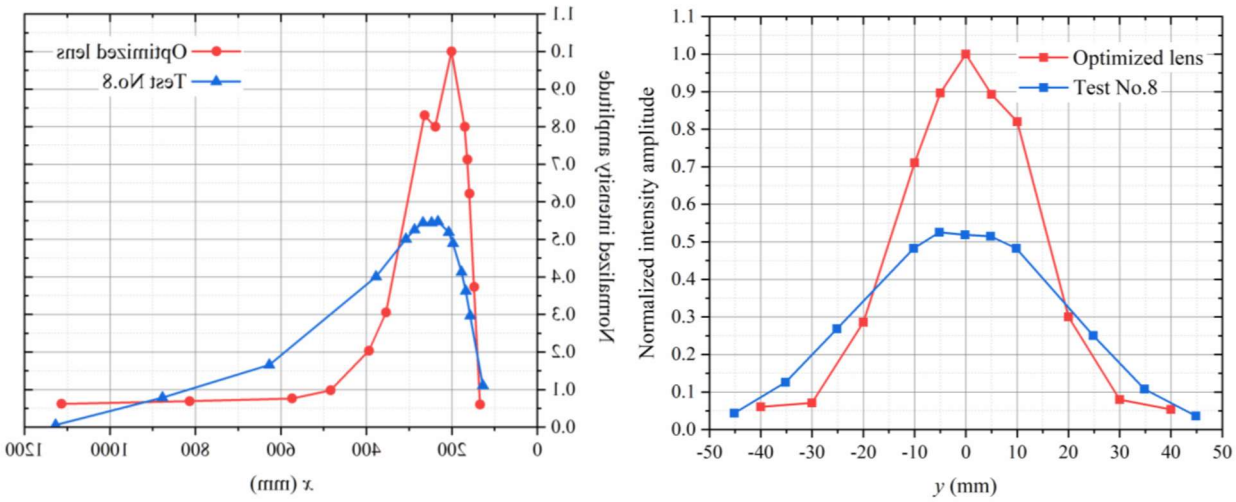

FIGURE 9. Normalized intensity amplitude along (a) *x*-axis and (b) *y*-axis for non-optimized (test No. 8) and optimized test.

To study the characteristics of the optimized test, other tests (Test No. 5, 8, 12) of the orthogonal table (Table II) can be selected as a comparison. Fig. 7 shows the simulation results for different tests. It is observed that the optimized test has the highest wave intensity M, and the lowest effective horizontal width L_h and vertical width L_v. Therefore, the result obtained from the optimized parameters of the orthogonal test meets our expectations and enables significant advantages over the unoptimized test. It should be noted that the focal length l_F is not considered in the optimal method, because different focal lengths should be determined in different applications. Therefore, it is necessary to first determine the expectation of l_F and then optimize the parameters using the methods above.

IV. EXPERIMENTS

An experiment is performed to verify the optimal results, and the wave intensities along the x-axis and y-axis of the acoustic composite lenses are measured. Fig. 8 shows the experimental setup, which includes the measurement and imaging system, and the experimental method is also shown. In the experiment, a 64-channel ultrasonic transmitting probe is used as the sound transmitting device, and an identical receiving probe is used to measure the sound field signal. The probe used in the experiment can excite ultrasound up to 5 MHz so that it can be used in this study. Moreover, the acoustic lens is placed at a reasonable position between the two probes to focus the incident ultrasonic waves. There are absorbers around the water tank to avoid the effects of reflected waves. In this work, 16 scans along the x-direction with 75 mm gaps

are selected to measure the acoustic field at different points, and the data received by each channel is transmitted to the host controller. For the probes in this experiment, water is selected as the officially specified impedance matching medium so that the best measurement results can be obtained in the underwater system.

V. CONCLUSION

In this work, the impact factors of an acoustic lens are investigated using a $L_{27}(3^8)$ orthogonal table. Finite element simulations are performed for different combinations of factors to obtain the wave intensity, focal area dimensions and focal length, which are selected as results in the test. Through the range analysis, the influence degree of each parameter on different results is obtained. For wave intensity M, the top three impact factors are P_0, c and k. Moreover, for effective horizontal width L_h and vertical width L_v, the top three impact factors are c, k, and b. And for focal length l_F, the order is k, c and a. For the biased angle of the incident wave, the concave depth r should be as small as possible to prevent focal intensity loss, and hexagonal structure has the best focusing performance. In this way, the structure of the acoustic lens is optimized. The experimental results show that the focusing intensity of the optimized acoustic lens is nearly 90% higher than the nonoptimized one, which proves the effectiveness of the orthogonal test optimization method in this paper.

REFERENCES

[1] A. Serkan, K. Olgun Adem, A. Baris Baykant, "Frequencycontrolled wave focusing by a sonic crystal lens," Appl. Acous. vol. 70, pp. 1400-1405, 2009.

[2] M. S. Kushwaha, P. Halevi, L. Dobrzynski, B. Djafari-Rouhani, "Acoustic band structure of periodic elastic composites," Phys. Rev. Lett. vol. 71, pp. 2022–2025, 1993.

[3] S. John, "Strong localization of photons in certain disordered dielectric superlattices," Phys. Rev. Lett. vol. 58, pp. 2486–2489, 1987.

[4] D. Schurig, J. J. Mock, B. J. Justice, S. A. Cummer, J. B. Pendry, A. F. Starr, D. R. Smith, "Metamaterial electromagnetic cloak at microwave frequencies," Science. vol. 314, pp. 977–980, 2006.

[5] N. Fang, D. Xi, J. Xu, M. Ambati, W. Srituravanich, C. Sun, X. Zhang, "Ultrasonic metamaterials with negative modulus," Nat. Mater. vol. 5, pp. 452–456, 2006.

[6] R. Martínez-Sala, J. Sancho, J. V. Sánchez, V. Gómez, J. Llinares, F. Meseguer, "Sound Attenuation by a Two sculpture," Nature. vol. 378, pp. 241, 1995.

[7] F. R. Montero de Espinosa, E. Jiménez, M. Torres, "Ultrasonic band gap in a periodic two dimensional composite," Phys. Rev. Lett. vol. 80, pp. 1208–1211, 1998.

[8] Ma, G. & Sheng, P., "Acoustic metamaterials: From local resonances to broad horizons," Sci. Adv. vol. 2 pp. e1501595, 2016.

[9] T. Brunet, A. Merlin, B. Mascaro, K. Zimny, J. Leng, O. Poncelet, C. Aristégui, O. Mondain-Monval, "Soft 3-D acoustic metamaterial with negative index," Nat. Mater. vol. 14, pp. 384–388, 2015.

[10] Shen, C. et al., "Broadband Acoustic Hyperbolic Metamaterial," Phys. Rev. Lett. vol. 115, pp. 254301, 2015.

[11] J. X. C., L. I. and Khuri-Yakub, "Surface Micromachined Capacitive Ultrasonic Immersion Transducers X. C. Jin, I. Ladabaum, B. T. Khuri-Yakub," IEEE Transactions on Ultrasonics, Ferroelectrics, and Frequency Control, vol. 45, pp. 678-690, 2002.

[12] T. C. Chang, M. J. Weber, M. L. Wang, J. Charthad, B. P. T. Khuri-Yakub, and A. Arbabian, "Design of Tunable Ultrasonic Receivers for Efficient Powering of Implantable Medical Devices With Reconfigurable Power Loads," IEEE Transactions on Ultrasonics, Ferroelectrics, and Frequency Control, vol. 63, pp. 1554-1562, 2016.

[13] V. F. Tseng, S. S. Bedair and N. Lazarus, "Phased Array Focusing for Acoustic Wireless Power Transfer," IEEE Transactions on Ultrasonics, Ferroelectrics, and Frequency Control, vol. 65, pp. 39- 49, 2018.

[14] R. A. Shelby, D. R. Smith, S. Schultz, "Experimental verification of a negative index of refraction," Science vol. 292, pp. 77–79, 2001.

[15] S. Zhang, L. Yin, N. Fang, "Focusing ultrasound with an acoustic metamaterial network," Phys. Rev. Lett. vol. 102, pp. 194301, 2009.

[16] Xie, Y. et al., "Acoustic Imaging with Metamaterial Luneburg Lenses," Sci. Rep. vol. 8, 2018.

[17] Chen, M., Jiang, H., Zhang, H., Li, D. & Wang, Y., "Design of an acoustic superlens using single-phase metamaterials with a starshaped lattice structure," Sci. Rep. vol. 8, 2018.I. Kamwa, R. Grondin, and D. Mcnabb, "On-line tracking of changing harmonics in stressed power systems: application to Hydro-Quebec network," *IEEE Transactions on Power Delivery*, vol. 11, no. 4, pp. 2020-2027, 1996.

[18] Dong, H., Zhao, S., Wang, Y. & Zhang, C., "Broadband singlephase hyperbolic elastic metamaterials for super-resolution imaging," Sci. Rep. vol. 8, 2018.

[19] Zhu, R., Liu, X. N., Hu, G. K., Sun, C. T. & Huang, G. L., "Negative refraction of elastic waves at the deep-subwavelength scale in a single-phase metamaterial," Nat. Commun. vol. 5, 2014.

[20] Sukhovich, A. et al., "Experimental and theoretical evidence for subwavelength imaging in phononic crystal," Phys. Rev. Lett. vol. 102, pp. 154301, 2009.

[21] Climente, A., Torrent, D. & Sánchez-Dehesa, J., "Sound focusing by gradient index sonic lenses," Appl. Phys. Lett. vol. 97, pp. 104103, 2010.

[22] Peng, S. et al., "Acoustic far-field focusing effect for twodimensional graded negative refractive-index sonic crystals," Appl. Phys. Lett. vol. 96, pp. 263502, 2010

[23] Lin, S. S., Huang, T. J., Jia-Hong, S. & Tsung-Tsong, W., "Gradient-index phononic crystals," Phys. Rev. B vol. 79, pp. 94302, 2009.

[24] Hu, X., Chan, C. T. & Zi, J., "Two-dimensional sonic crystals with Helmholtz resonators," Phys. Rev. E vol. 71, pp. 55601, 2005.

[25] Yang, X., Yin, J., Yu, G., Peng, L. & Wang, N., "Acoustic superlens using Helmholtz-resonator-based metamaterials," Appl. Phys. Lett. vol. 107, pp. 193505, 2015.

[26] X. Cai, Q. Guo, G. Hu, J. Yang, "Ultrathin low-frequency sound absorbing panels based on coplanar spiral tubes or coplanar Helmholtz resonators," Appl. Phys. Lett. vol. 105, pp. 121901, 2014.

[27] Popa, B. & Cummer, S. A., "Design and characterization of broadband acoustic composite metamaterials," Phys. Rev. B vol. 80, 2009.

[28] Zigoneanu, L., Popa, B. & Cummer, S. A., "Design and measurements of a broadband two-dimensional acoustic lens," Phys. Rev. B vol. 84, 2011.

[29] Yongdu, R. et al., "3-D underwater acoustic wave focusing by periodic structure," Appl. Phys. Lett. vol. 114, pp. 81908, 2019.

[30] Sanchis, L., Yánez, A., Galindo, P. L., Pizarro, J. & Pastor, J. M., "3-D acoustic lenses with axial symmetry," Appl. Phys. Lett. vol. 97, pp. 54103, 2010.

[31] Sánchez-Pérez, J. V. et al., "Sound Attenuation by a Two- Dimensional Array of Rigid Cylinders," Phys. Rev. Lett. vol. 80, pp. 5325, 1998.

[32] Hakansson A, Sanchez-Dehesa J. "Acoustic lens design by genetic algorithms," Phys, Rev. B vol. 7021, pp. 214302, 2004.

[33] Li D, Zigoneanu L, Popa B, Cummer S A. "Design of an acoustic metamaterial lens using genetic algorithms," J. Acoust. Soc. Am. vol. 1324, pp. 2823-2833, 2012.

[34] Fokin, V., Ambati, M., Sun, C. & Zhang, X., "Method for retrieving effective properties of locally resonant acoustic metamaterials," Phys. Rev. B vol. 76, 2007.

[35] Wu, L. & Chen, L., "Acoustic band gaps of the woodpile sonic crystal with the simple cubic lattice," J. Phys. D Appl. Phys. vol. 44, pp. 45402, 2011.

[36] Xiaojuan J , Qi O . "Optimal Design of Point-focusing Shear Vertical Wave Electromagnetic Ultrasonic Transducers based on Orthogonal Test Method," IEEE Sens. J. vol. 18, pp. 8064-8073, 2018.

[37] J. Peng et al., "Orthogonal test design for optimization of supercritical fluid extraction of daphnoretin, 7-methoxy-daphnoretin and 1,5-diphenyl-1-pentanone from Stellera chamaejasme L. and subsequent isolation by high-speed counter-current chromatography," J. Chromatogr. A, vol. 1135, pp. 151–157, 2006.

[38] Elford, D. P., Chalmers, L., Kusmartsev, F. V. & Swallowe, G. M., "Matryoshka locally resonant sonic crystal," J. Acoust. Soc. Am. vol. 130, pp. 2746, 2011.